

## Supporting Information

© Copyright Wiley-VCH Verlag GmbH & Co. KGaA, 69451 Weinheim, 2013

### **Studies on the MxiH Protein in T3SS Needles Using DNP-Enhanced ssNMR Spectroscopy**

Pascal Fricke, Jean-Philippe Demers, Stefan Becker, and Adam Lange<sup>\*[a]</sup>

cphc\_201300994\_sm\_miscellaneous\_information.pdf

## Supporting Information

### Experimental details for the acquisition of the NMR spectra

For the initial cross-polarization (CP) transfer step from  $^1\text{H}$  to  $^{13}\text{C}$ , a ramped CP (from 100 % to 80 %) with a contact time of 0.4 ms (0.2 ms in case of  $^{13}\text{C}$ - $^{13}\text{C}$  SPC-5<sup>[1]</sup>) was used. The initial CP contact time from  $^1\text{H}$  to  $^{15}\text{N}$  was set to 0.2 ms.

For all experiments, the proton decoupling during the acquisition and evolution times was carried out using an r.f. field strength of 83.3 kHz and the SPINAL-64<sup>[2]</sup> decoupling scheme. During the N-C SPECIFIC-CP<sup>[3]</sup> steps in the triple resonance experiments continuous wave (CW) proton decoupling with an r.f. field amplitude of 83.3 kHz was employed. The CW proton decoupling during the SPC-5 recoupling blocks was carried out using 110 kHz of r.f. field amplitude.

All experiments were conducted using 2 dummy scans and a recycle delay of 2 s. The 2D and 3D NMR spectra were acquired in a phase-sensitive manner using TPPI. Further acquisition parameters and experimental times can be found in Table S1.

Before Fourier transform, the acquired points were zero-filled and window functions were applied. The corresponding parameters are given in Table S2.

**Table S1.** Overview of acquisition parameters and experimental times. “F1” refers to the direct dimension, whereas “F2” and “F3” refer to the indirect dimensions. “ns” refers to the number of scans.

Experiment	Mixing elements (duration)	Acquisition time / ms (points)				
		F1 ( $^{13}\text{C}$ )	F2 ( $^{13}\text{C}/^{15}\text{N}$ )	F3 ( $^{15}\text{N}$ )	ns	Total time
$^1\text{H}$ - $^{13}\text{C}$ CP 1D	N/A	10.6 (1024)	N/A	N/A	128	4 min
$^{13}\text{C}$ - $^{13}\text{C}$ 2D	PDSD (20 ms) <sup>[4]</sup>	10.6 (1024)	10.6 (1024)	N/A	22	13 h 58 min
$^{13}\text{C}$ - $^{13}\text{C}$ 2D	SPC-5 (0.4 ms excit./reconv. each)	9.3 (894)	3.2 (352)	N/A	64	12 h 40 min
NCA 2D	SPECIFIC-CP (3.0 ms)	9.3 (894)	12.0 (73)	N/A	128	6 h 33 min
NCO 2D	SPECIFIC-CP (3.0 ms)	9.3 (894)	12.0 (73)	N/A	128	6 h 33 min
NCACX 2D	SPECIFIC-CP (3.0 ms), PDSD (20 ms)	9.3 (894)	12.0 (73)	N/A	128	6 h 36 min
NCACX 3D	SPECIFIC-CP (3.0 ms), PDSD (20 ms)	9.3 (894)	8.0 (83)	5.1 (25)	64	3 d 3 h 30 min
NCOCX 2D	SPECIFIC-CP (3.0 ms), PDSD (50 ms)	9.3 (894)	12.0 (73)	N/A	128	6 h 41 min
NCOCX 3D	SPECIFIC-CP (3.0 ms), PDSD (50 ms)	9.3 (894)	8.1 (51)	5.1 (25)	96	3 d 4 h 36 min

**Table S2.** Overview of processing parameters. “F1” refers to the direct dimension, whereas “F2” and “F3” refer to the indirect dimensions. The  $\phi$ -angle defines the phase shift of the squared sine window function.

Experiment	Points after FT			Window function		
	F1( $^{13}\text{C}$ )	F2( $^{13}\text{C}/^{15}\text{N}$ )	F3( $^{15}\text{N}$ )	F1 ( $^{13}\text{C}$ )	F2 ( $^{13}\text{C}/^{15}\text{N}$ )	F3 ( $^{15}\text{N}$ )
$^1\text{H}$ - $^{13}\text{C}$ CP 1D	16 K	N/A	N/A	none	N/A	N/A
$^{13}\text{C}$ - $^{13}\text{C}$ 2D (PDSD)	2 K	2 K	N/A	$\sin^2, \phi=45^\circ$	$\sin^2, \phi=45^\circ$	N/A
$^{13}\text{C}$ - $^{13}\text{C}$ 2D (SPC-5)	2 K	2 K	N/A	$\sin^2, \phi=45^\circ$	$\sin^2, \phi=45^\circ$	N/A
NCA 2D	2 K	256	N/A	$\sin^2, \phi=48.6^\circ$	$\sin^2, \phi=48.6^\circ$	N/A
NCO 2D	2 K	256	N/A	$\sin^2, \phi=45^\circ$	$\sin^2, \phi=45^\circ$	N/A
NCACX 2D	2 K	1 K	N/A	$\sin^2, \phi=45^\circ$	$\sin^2, \phi=45^\circ$	N/A
NCACX 3D	1 K	128	128	$\sin^2, \phi=45^\circ$	$\sin^2, \phi=56.3^\circ$	$\sin^2, \phi=56.3^\circ$
NCOCX 2D	2 K	1 K	N/A	$\sin^2, \phi=45^\circ$	$\sin^2, \phi=45^\circ$	N/A
NCOCX 3D	1 K	128	128	$\sin^2, \phi=45^\circ$	$\sin^2, \phi=56.3^\circ$	$\sin^2, \phi=56.3^\circ$

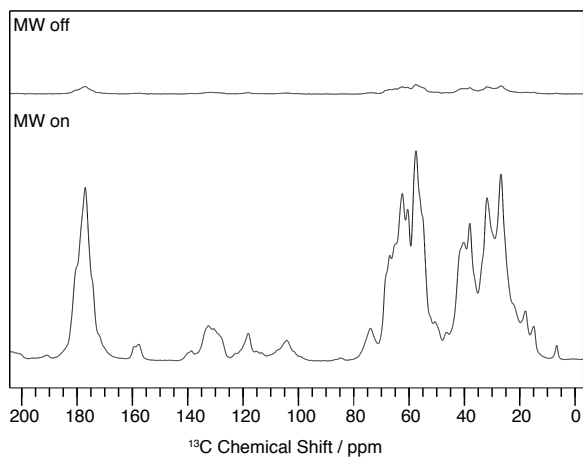


**Figure S1.** Comparison of the  $^1\text{H}$ - $^{13}\text{C}$  CP 1D NMR spectra with microwaves switched on/off. The signals were about 23 times stronger when the sample was irradiated with microwaves.

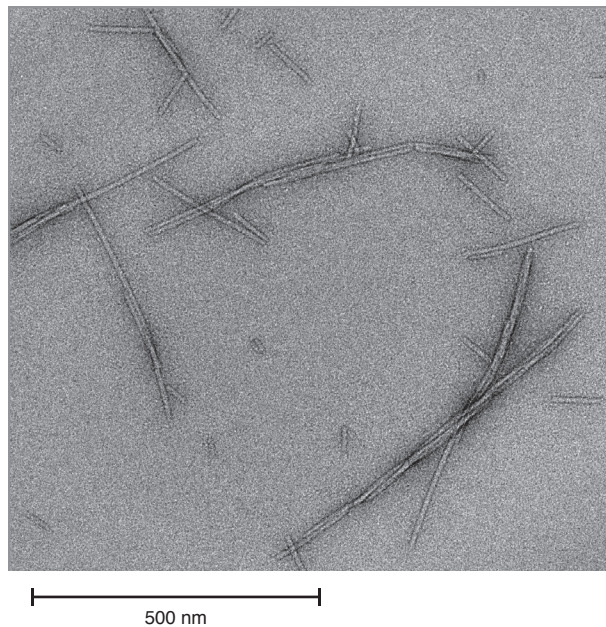


**Figure S2.** Transmission electron microscopy image of the ssNMR needle sample taken after the collection of all NMR data for this study. The presence of the needles confirms that they were not destroyed or altered by cryogenic freezing in the glycerol/water matrix or by microwave irradiation.

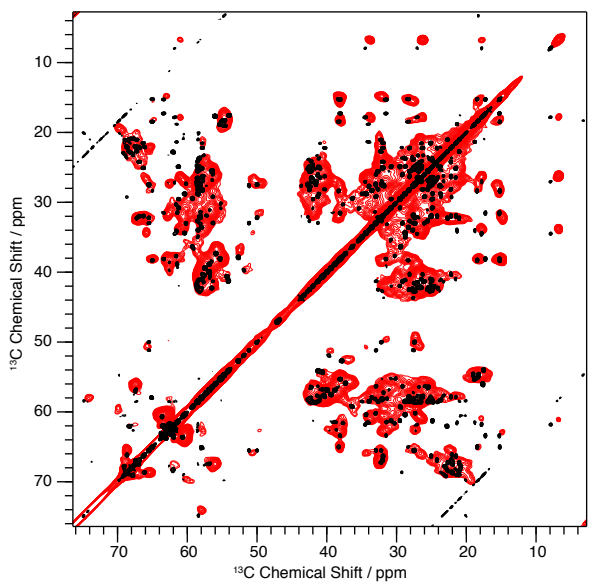


**Figure S3.** Overlay of the  $^{13}\text{C}$ - $^{13}\text{C}$  PDSD 2D NMR spectrum acquired on a 20.0 T NMR magnet (corresponding  $^1\text{H}$  Larmor frequency: 850 MHz) at ambient temperature (in black) with the  $^{13}\text{C}$ - $^{13}\text{C}$  PDSD 2D NMR spectrum acquired on the 14.1 T NMR DNP setup (corresponding  $^1\text{H}$  Larmor frequency: 600 MHz) at cryogenic temperature (104 K) (in red). Please note that the higher resolution at ambient temperature also arises from the considerably higher magnetic field strength.

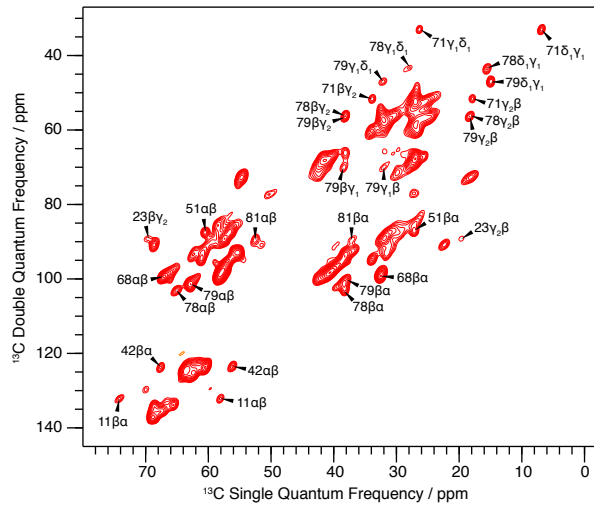


**Figure S4.**  $^{13}\text{C}$ - $^{13}\text{C}$  SPC-5 2D NMR spectrum with assignments.

**Table S3.** Chemical shifts (in ppm relative to DSS) of the resonances that could be assigned. Deviations from the known resonances at ambient temperature<sup>[5]</sup> are highlighted (> 1 ppm in yellow, > 3 ppm in red).

		N	C'	C $\alpha$	C $\beta$	C $\gamma$	C $\delta$	C $\epsilon$
4	Thr			61.9	67.9			
5	Val			68.2	28.8			
7	Asp	119.3		55.0	41.1			
9	Asp	119.1		55.0	40.1			
11	Thr	108.5	176.0	57.9	74.0	21.1		
15	Leu	129.7	178.0	58.0	40.6	27.3	27.3	27.3
20	Asp	120.7		57.6	40.2			
21	Asp	120.7	179.2	57.6	40.3			
22	Gly	112.2	176.1	46.9				
23	Thr	106.4		59.8	69.8	19.5		
26	Leu	124.7	178.5	57.2	40.0	31.7	24.2	26.9
28	Gly		178.4	46.6				
29	Gln	121.0		59.2	27.3	35.6		
31	Thr	120.6	176.2	67.1	68.9	22.3		
32	Ser	118.5						
40	Asn	119.4	170.3	49.2	38.4			
41	Pro			62.6	31.5	27.3	49.7	
42	Ser	106.1	174.1	56.0	67.5			
43	Asn	125.8	171.3	51.2	39.6	176.0		
44	Pro			65.9	34.3	26.8	50.6	
45	Gln	116.6	181.7	58.5	27.1	31.0		
46	Leu	122.0						
48	Ala	123.6	182.4	55.2	19.0			
49	Glu	121.0	179.9	59.1	28.8	35.9	184.0	
50	Tyr	118.9	177.0	62.8	39.3		131.7	118.3
51	Gln	116.7	181.4	60.5	26.9	32.0	177.4	
52	Ser	119.2	175.8	64.0	60.5			
53	Lys	126.1						
58	Thr	108.0	177.0	65.5	68.6	22.3		
60	Tyr	124.4	177.0	58.5	37.4			
61	Arg	117.6	180.8	56.4	31.4	25.4	41.8	
62	Asn	120.8						
64	Gln	122.6	175.5	57.3	31.9	33.5	179.7	
65	Ser	110.3	179.5	60.3	63.4			
66	Asn	118.5	176.6	55.7	36.8	174.3		
67	Thr	117.4	174.5	69.0				
68	Val	120.9	176.5	67.1	32.4	21.1		23.7
69	Lys	119.3						
70	Val	118.5	180.9	67.1	31.8	24.4		
71	Ile	117.9	177.5	61.0	33.8	26.3	6.8	17.8
72	Lys	124.2						
74	Val	124.3		66.4	32.3	25.5		
75	Asp	118.9	177.0	54.9	38.0	172.0		
76	Ala	122.3	180.4	54.5	18.0			
77	Ala	122.3	180.5	54.5	18.0			
78	Ile	121.8	178.3	65.1	38.1	18.3	15.4	27.9
79	Ile	116.7	180.4	62.8	38.2	18.3	14.9	
						32.1		
81	Asn	117.0	175.0	52.5	37.0			
82	Phe	118.0						

## References (Supporting Information)

- [1] M. Hohwy, C. M. Rienstra, C. P. Jaroniec, R. G. Griffin, *J. Chem. Phys.* **1999**, *110*, 7983-7992
- [2] B. M. Fung, A. K. Khitrin, K. Ermolaev, *J. Magn. Reson.* **2000**, *142*, 97-101
- [3] M. Baldus, A. T. Petkova, J. Herzfeld, R. G. Griffin, *Mol. Phys.* **1998**, *95*, 1197-1207
- [4] N. M. Szevernyi, M. J. Sullivan, G. E. Maciel, *J. Magn. Reson.* **1982**, *47*, 462-475
- [5] J. P. Demers, N. G. Sgourakis, R. Gupta, A. Loquet, K. Giller, D. Riedel, B. Laube, M. Kolbe, D. Baker, S. Becker, A. Lange, *PLoS Pathog.* **2013**, *9*, e1003245